Researchers Journal of Science and Technology (REJOST)
https://rejost.com.ng

Predictive Analysis of Sand Production and Flow Implications using Petrophysical-Geomechanical Properties: A case of "ANY" Field, Niger Delta

[1]Ekefre, Anyanime Edet, [2]George, Nyakno Jimmy, [1]Udoh, Abraham Christopher,[1]Thomas Akpan Harry, & [1]Etim, Camillus Eyo

Received: January 21, 2025 /Accepted: March 22, 2025

Abstract

A predictive analysis of sand production and flow implications using petrophysical-geomechanical properties: A case of the 'ANY' field, Niger Delta, was carried out. Datasets, including well logs and 3-D seismic, were used to investigate the geomechanical properties of the field and predict sand production based on the results obtained. Sand production is expected because the Niger Delta Province is predominantly a loose sandstone terrain, and the sand grains are highly friable. The study centers on employing empirical relationships of rock mechanical parameters from wireline logs to predict the vulnerability of the reservoir formations to sand production. The four reservoir units (A1, A2, A3, and A4) were first recognized by using wireline logs (gamma ray), and the fluids were differentiated using resistivity, neutron porosity, and density logs. We correlated the identified hydrocarbon prospecting sands across all three wells. Shear and compressive waves from the sonic log were then used to derive the rock mechanical parameters (Poisson ratio (ν), Young modulus (E), shear/rigidity modulus (G), bulk modulus (Kb), bulk compressibility (Cb), and unconfined compression strength (UCS)). Five sand production methods (porosity, acoustic wave travel time, sand production index (B), Schlumberger sand production index (SI), shear modulus to bulk compressibility ratio (G/Cb)) derived from the rock mechanical parameters were used to adequately analyze sanding. The analyzed reservoir exhibits sandstone units with a higher average value range

of Poisson ratio, bulk modulus, Young's modulus, shear modulus, and unconfined compression strength of 0.26 to 0.33, 15.29 to 20.90 MPa, 15.52 to 29.23 MPa, 5.84 to 11.56 MPa, and 22.45 to 29.23, respectively. The reservoirs exhibited higher values of the Poisson ratio, indicative of their ductile nature that is resulting from shale intercalations, which is evident in the moderate net to gross (NTG) ratio, leading to enhanced stiffness due to elevated moduli, hence less prone to deformation. The results of the five (5) predictions of sand production models indicate a very low risk of sanding during production of the investigated reservoirs. Thus, this research application of empirical relationships derived from rock mechanical parameters and wireline logs in predicting sand production has effectively deduced that the reservoirs in ANY field were highly compacted and consolidated, and therefore problems associated with sand production (sanding) during hydrocarbon extraction in this field are ruled out or almost unlikely.

✉ Ekefre, Anyanime Edet: ekefreanyanime@gmail.com

[1]Department of Geology, Akwa Ibom State University, Mkpat Enin, Uyo, PMB 1162, Nigeria
[2]Department of Physics (Geophysics Research Group), Akwa Ibom State University, Mkpat Enin, Uyo, PMB 1162, Nigeria

Keywords: Sand production, Petrophysical properties, Geomechanical properties, Niger Delta, Wireline logs

1.0 Background of Study

Sand production is a critical issue in the oil and gas industry, particularly in weakly consolidated and unconsolidated reservoirs, such as those found in the Niger Delta. It occurs when the reservoir rock collapses due to mechanical stress during hydrocarbon production, leading to the migration of sand particles into the wellbore (Santarelli & Carminati, 1995). The consequences of sand production include wellbore instability, damage to production equipment, reduced hydrocarbon flow, and increased operational costs. The Niger Delta is characterized by complex depositional environments and heterogeneous reservoir properties. These reservoirs, predominantly composed of unconsolidated sandstone, are highly prone to sand production due to their low rock strength and high permeability (Adeoye *et al*., 2020). The interplay of petrophysical properties such as porosity, permeability, and grain size distribution with geomechanical parameters like in-situ stress, rock strength, and pore pressure significantly influences sand production potential (Osia *et al*., 2020). In the context of the ANY Field, a deeper understanding of the relationship between petrophysical and geomechanical properties and their impact on sand production is essential. Integrating well log data with seismic analysis provides a robust framework for identifying high-risk zones, optimizing production, and designing effective sand control measures (Ibrahim *et al*., 2021). Traditionally, sand production has been managed proactively through mechanical and chemical sand control methods. However, these methods are often costly and may not fully address the problem. A proactive approach involving predictive modeling can identify sand-prone zones and inform reservoir management strategies. This study aims to leverage the integration of petrophysical and geomechanical parameters derived from well logs and seismic data to predict sand production in the ANY Field, Niger Delta, ultimately improving reservoir management and production efficiency.

2.0 Location and Geology of the Study Area

This study area is located in the southeastern shallow offshore Niger Delta, about 60 km from the shoreline and with a water depth of 30 meters. The field is situated in the shallow offshore depobelts (Figure 1), and the well locations are shown in Figure 2. The Niger Delta's tectonic evolution began with the

separation of the African and South American plates during the Late Jurassic, forming a triple junction rift-ridge system. This system consisted of the Atlantic arm, the Gulf of Guinea transform complex, and the Abakaliki-Benue Trough, the Oldest Sedimentary Basin. Rifting ceased in the Late Cretaceous, leading to gravity-driven tectonism, which shaped the Niger Delta Basin (Tuttle *et al*., 1999). The stratigraphy of the Niger Delta consists of three main formations: Akata, Agbada, and Benin (Short & Stauble, 1967; George et al., 2022). The Akata Formation (Eocene–Recent) is composed mainly of marine shales with sandy interbeds; it serves as the primary source rock for hydrocarbons (Akpan *et al*., 2022a). Its thickness ranges from 600 m to over 6000 m (Weber & Daukoru, 1975). The Agbada Formation (Eocene–Oligocene) is a mix of sandstones, shales, and siltstones, with the upper sandy unit acting as the main hydrocarbon reservoir (Horsfal *et al*., 2024). Its unconsolidated nature causes geomechanical challenges. Thickness ranges from 300 m to 4500 m (Weber & Daukoru, 1975), while the Benin Formation (Miocene–Recent) is the youngest unit, consisting mainly of non-marine sands and gravels, forming the primary aquifer for potable water. It has minimal hydrocarbon presence and a thickness of about 2100 m (Weber & Daukoru, 1975).

3.0 Materials and Methods

3.1 Materials

The datasets used in this study include post-stacked 3-D seismic data, digitized logs in LAS format (including gamma ray, acoustic, density, neutron, and resistivity), check shots, and deviation statistics data. These datasets were analyzed and interpreted using Schlumberger Petrel, interactive petrophysics, and Microsoft Excel.

3.2 Methodology

The approach developed for this investigation aids in the optimization of the geomechanical and petrophysical evaluation of "ANY" reservoirs (Figure 3). The detailed process consists of geo-mechanic estimation for the mechanical rock properties and the formation strength to support completion design, seismic interpretation to provide lateral resolution of the subsurface, and petrophysical evaluation to provide vertical resolution properties of wellbore.

3.3 Data Loading

The data loading process into Petrel begins with importing wellheads, which include well names, surface positions, Kelly bushing, top depth, and bottom depth for accurate placement on the base map. Check shot, deviation, and log data (gamma ray, resistivity, density, porosity, water saturation, and shale volume) are then imported. Finally, seismic volumes are loaded in SEG-Y format.

3.4 Well Normalization

Well normalization standardizes log data across multiple wells to ensure consistency in subsurface modeling and reservoir characterization (Ebong *et al*., 2023). It corrects variations caused by logging conditions, operations, or measurement units. The logs were scaled as follows: gamma ray (0–150 API), resistivity (0.2–2000 ohm-m), density (1.65–2.65 g/cm^3), neutron porosity (0–0.6), and sonic (40–140 µsec/ft). Each log track was assigned a distinct color.

3.5 Reservoir Identification / Well Correlation

The process involves identifying and correlating formation tops to establish a chronostratigraphic framework. Wells were arranged along strike lines (A to A') based on their location and relative distances. Sand bodies were identified using the gamma ray log and correlated to adjacent wells to ensure lateral continuity of identified sand intervals across the three wells using gamma ray logs for lithology and resistivity logs to determine fluid content (hydrocarbon or water).

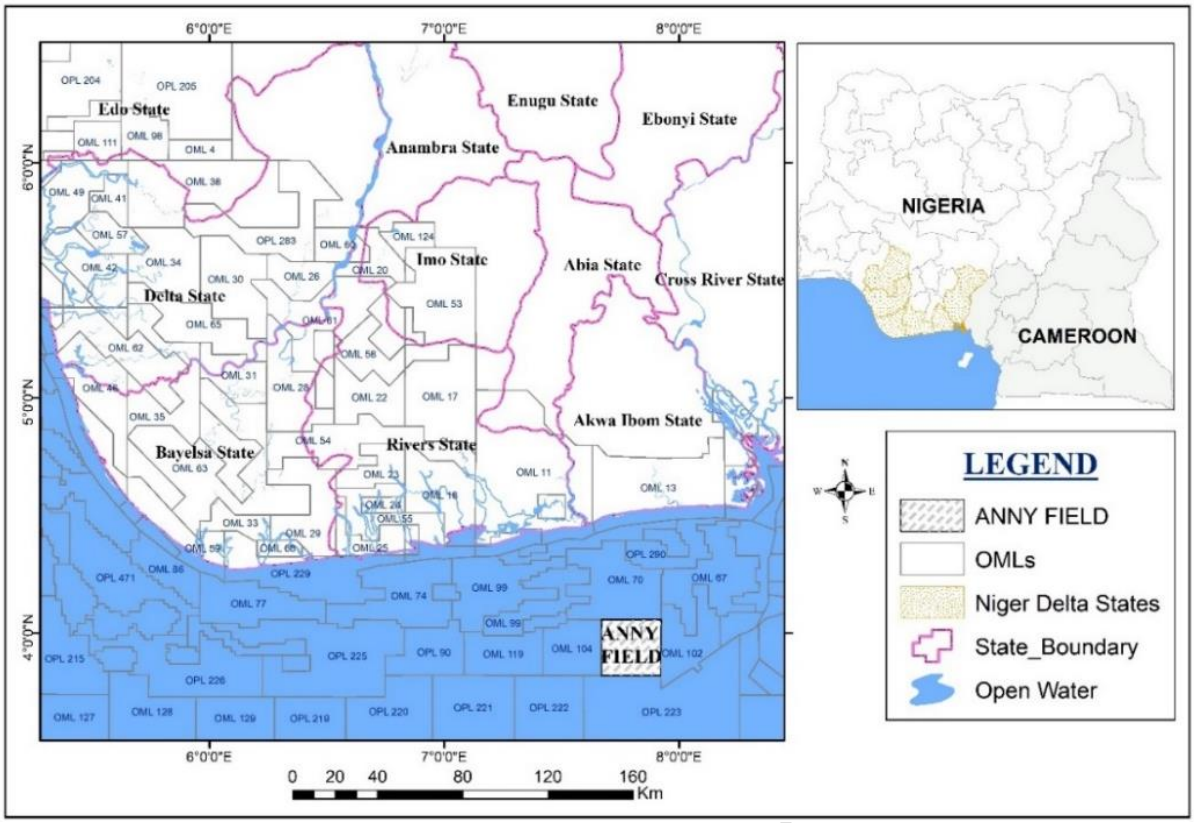

Figure 1: Map of Niger Delta showing the study area

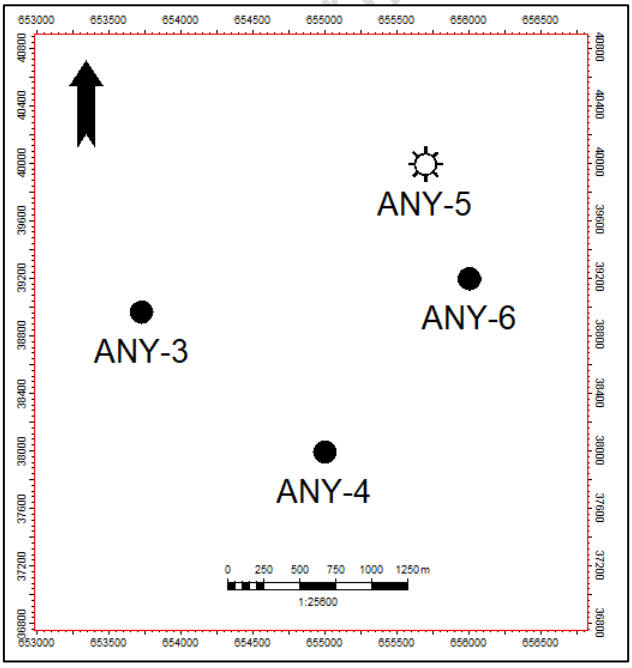

Figure 2: Base map of the study area showing well locations

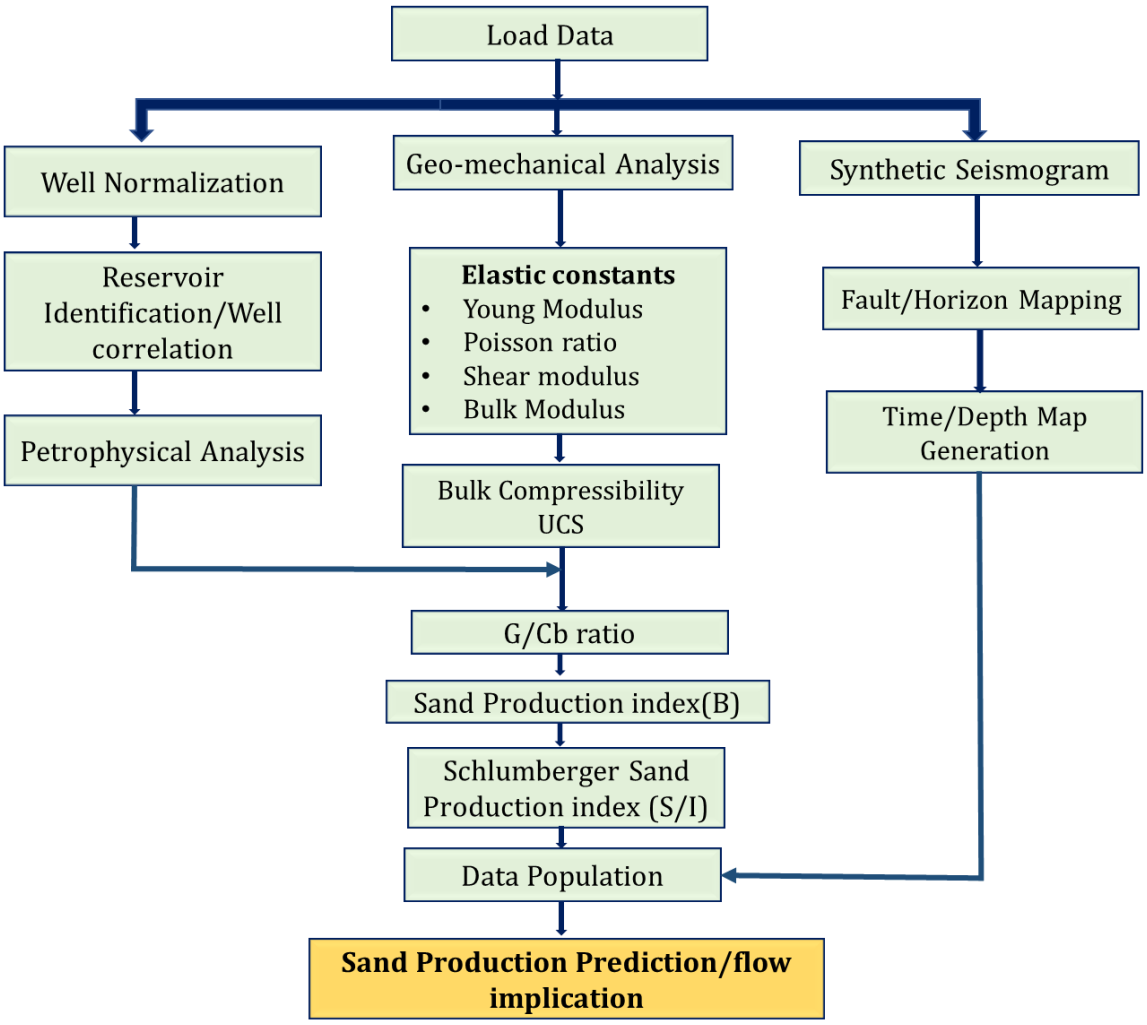

Figure 3: Workflow design for the study

3.6 Petrophysical Analysis

Petrophysical analysis evaluates well log data to determine key reservoir properties such as porosity, permeability, water saturation, and hydrocarbon saturation. These parameters help assess the reservoir's storage and fluid flow capabilities. The study estimated sand thickness, shale content, bulk volume water, hydrocarbon pore volume, and net pay.

3.6.1 Gross and Net Sand Thickness

Gross sand thickness represents the total sand section in a well, including both productive and non-productive zones, while net sand thickness accounts only for the reservoir-quality sands (Akpan et al., 2022b). Net thickness was determined by applying cutoff values for porosity (>12%), permeability (>50 mD), shale volume (<30%), and hydrocarbon saturation (>50%). The net-to-gross ratio (NTG) was calculated to assess reservoir productivity. The net-to-gross ratio was determined using equation 1 below:

$$NTG = \frac{Net\ Thickness}{Gross\ Thickness} \quad 1$$

3.6.2 Porosity

Porosity is the fraction of rock volume occupied by pore spaces; it is crucial for determining fluid storage capacity and was estimated by inputting the bulk density measurements acquired from the density log within each reservoir into equation 2**.**

$$\emptyset_T = \frac{\rho_{mat} - \rho_{bulk}}{\rho_{mat} - \rho_{fluid}} \quad 2$$

where ρ_{mat} is the density of rock matrix, ρ_{bulk} is the bulk density and ρ_{fluid} is the fluid density

3.6.3 Shale Volume

Shale volume (Vsh) helps distinguish clean reservoir sands from shaly intervals. It was estimated using the gamma-ray (GR) log in equation 3. The Gamma Ray Index (IGR) is shown as:

$$I_{GR} = \frac{GR_{log} - GR_{min}}{GR_{max} - GR_{min}} \quad 3$$

3.6.4 Water Saturation

Water saturation (Sw) indicates the fraction of pore space filled with formation water, influencing hydrocarbon saturation and production potential. Water saturation was calculated using the Archie's formula given in equation 4.

$$S_w^n = \frac{a}{\emptyset^m} \cdot \frac{R_w}{R_t} \quad 4$$

where: Sw is water saturation, Rw is the formation water resistivity, Rt is the true formation resistivity, ϕ is Porosity, a is tortuosity factor (1), m is cementation exponent (typically 1.8 – 2.0 for sandstones) and n is saturation exponent (typically 2.0 for water-wet rocks).

3.6.5 Permeability

Permeability (k) measures a rock's ability to transmit fluids and is crucial for reservoir performance evaluation. In the absence of core data, equation 5, known as Timur's Equation, provides an estimation:

$$k = 0.136 \times \emptyset^4 \times S_{wirr}^{-2} \quad 5$$

where S_{wirr} is the Irreducible water saturation and ∅ is Porosity

3.7 Seismic Interpretation

Seismic interpretation is essential for subsurface exploration, providing a three-dimensional view of geological structures, stratigraphy, and rock properties (Vail, 1987). Unlike wellbore data, seismic data offers a broader understanding of subsurface complexity. To generate the synthetic Seismogram, **t**he sonic log was calibrated using check shot data to improve accuracy. The calibrated sonic log and density log were used to generate an acoustic impedance (AI) log, which was then used to create a reflectivity coefficient (RC) log. The RC log was convolved with a seismic wavelet to generate a synthetic seismogram, aiding in seismic-to-well correlation, which ensures alignment between seismic data and well logs, improving seismic interpretation accuracy by linking seismic reflectors to geological horizons (Vail, 1987). Faults were identified based on seismic reflection patterns, such as abrupt terminations, lateral velocity changes, and structural deformations. A variance attribute was used to enhance fault visibility, ensuring accuracy in complex fault systems. Stratigraphic horizons for the four reservoirs were mapped at 5 msec intervals across seismic lines to establish the field's stratigraphic framework. Time and depth structural maps were generated from mapped horizons to evaluate hydrocarbon-bearing zones, aiding in geological interpretation and reservoir assessment.

3.8 Geomechanical Properties Estimation

3.8.1 P-Wave velocity and S- Wave velocity

To determine compressional velocity or P-wave velocity (vp), the sonic interval time from sonic log was used. Sonic log data comprised the interval transit time, which is defined as the time necessary for elastic waves (compressional) to travel 1ft of the formation. The log data were recorded in μsec/ft. The interval transit times were transformed to compressional velocity in m/s, using the equation 6 (Ogagarue, 2008). relationship expressed as:

$$V_p = \frac{1000000 * 0.305}{\Delta t_p} \quad 6$$

where Δt_p is the interval transit times recorded by the compressional sonic logs, respectively, in μsec/ft and the (1000000*0.305) is the conversion factor from microseconds per foot (μsec/ft) to meters per second (m/s). An empirical relationship was used to calculate the

shear velocity, or S-wave velocity (V_s), from V_p as shown in equation 7.

$$V_s = \frac{V_p - 1279.08}{1.22702} \quad 7$$

Geomechanical properties were determined using well log data. The geomechanical properties include Poisson's ratio (v), Young's Modulus (E), Shear Modulus (G), Bulk Modulus (K), Bulk Compressibility (Cb), and Unconfined Compressive Strength (UCS).

3.8.2 Determination of Poisons Ratio (v)

Poisson's ratio **(v)** describes the measure of the geometric change of shape or the ratio of the lateral change (contraction) to longitudinal dilation. It is a plastic modulus. The log-derived Poisson ratio was calculated using the vp and vs relationship given in equation 8.

$$\text{Poisson's ratio } (\nu) = \frac{V_p^2 - 2V_s^2}{2(V_p^2 - V_s^2)} \quad 8$$

where Vp is the p-wave velocity and Vs is shear wave velocity. The theoretical maximum value of v = 0.5.

3.8.3 Determination of Young's Modulus (E)

Young's Modulus (E) defines the ratio of tensile or compressive stress to the resultant strain. The log derived Young's Modulus (E) was calculated using Vp and Vs relationship expressed in equation 9.

$$E = \rho V_s^2 \left(\frac{3V_p^2 - 4V_s^2}{V_p^2 - V_s^2} \right) \quad 9$$

where ρ = bulk density, vp = p-wave velocity, vs = S - wave velocity

3.8.4 Determination of Shear Modulus (G)

Shear Modulus (G**)** It is a rigidity modulus defined as the ratio of shearing stress to shear strain. The shear modulus of the reservoir was calculated using equation 10.

$$G = \rho V_s^2 \quad 10$$

where: ρ = Density and Vs = Shear wave velocity.

3.8.5 Determination of Bulk Modulus (K)

Bulk Modulus (K) describes or defines the response of an object to the change in volume under hydrostatic pressure or compression. Bulk modulus was calculated using the relationship between Poisson's ratio and Young's modulus. The formula is shown in equation 11.

$$K = \frac{E}{3(1-2v)} \quad 11$$

where: E = Young Modulus and v = Poisson's ratio.

3.8.6 Determination Bulk Compressibility (C_b)

Bulk compressibility was determined using the equation 12.

$$C_b = \frac{1}{K} \quad 12$$

where: K = Bulk Modulus

3.8.7 Unconfined Compressive Strength (UCS)

The UCS can be estimated using Young Modulus and empirical correlations. Equation 13 was used to calculate the UCS of the reservoir.

$$UCS = k.E \quad 13$$

where: E = Young Modulus and k is a constant, usually 0.03 for Sandstone (Barefield *et al.*, 2006).

3.9 Sand Production Prediction

Sand production poses a major challenge in hydrocarbon extraction, especially in reservoirs that are unconsolidated or weakly cemented. It occurs when reservoir rock fails due to mechanical stresses during production, causing sand particles to migrate into the wellbore. Predicting sand production is critical for optimizing production, ensuring wellbore stability, and minimizing equipment damage. The prediction of sand production was conducted using the methodology outlined below:

3.9.1 Shear Modulus to Bulk Compressibility Ratio (G/C_b)

The value for this method was calculated using the formula the ration, $\frac{G}{C_b}$, where G is the Shear modulus and $C_b$is the Bulk compressibility.

3.9.2 Sand Production Index (B) Method

Using this method to predicting sand production in a reservoir, equation 14 given below was used, using Young's modulus and Poisson's ratio.

$$B = \frac{E}{1-v^2} \qquad 14$$

where B is the sand production index method, E is the Young's modulus and v is the Poisson's ratio.

3.9.3 Schlumberger Sand Production Index (SI) Method

The Schlumberger sand production index method was calculated using equation 15.

$$SI = K \times G \qquad 15$$

where K is the bulk modulus and G is the Shear modulus.

3.10 Populating Sand Prediction Parameters

Populating attributes derived from well logs onto a seismic surface is a critical step in integrating well and seismic data for surface characterization. The calculated sand production parameters were then extrapolated across the reservoir surfaces to assess the likelihood of sanding throughout the reservoir.

4.1 Reservoir Identification & Well Correlation

The wells were arranged along strike line A to A' to depict the West to East position of each well across "ANY" field (Figure 4.1). After close geologic scrutiny of the three wells, sand horizons thatmeet all attributes to be called a reservoir were mapped on well ANY-3 and correlated across the adjacent wells. The lithological and stratigraphic study of the reservoir using the GR log shows that the geological units are predominantly sand and shale with an increasing trend of a high sand/shale ratio, confirming the area of interest to be within the Agbada Formation of the Niger Delta as shown in Figure 4.1. The correlation revealed four stacks of sand units in the reservoir, namelyA1, A2, A3, and A4, across the three wells. The lateral variation in reservoir thickness, which tends to be thickest at ANY-3, is strongly controlled by differential subsidence variation from the compaction of sediments and the presence of growth faults, as indicated in the Niger Delta. The reservoirs are located at a depth of 7200 ft to 11500 ft across the three wells.

4.2 Petrophysical Analysis

Populating attributes derived from well logs onto a seismic surface is a critical step in the petrophysical properties of the reservoirs. Table 1 and Figure 5 provide the critical insights into the potential for sand production. The Net-to-Gross (NTG) values indicate the proportion of reservoir-quality sand relative to the total interval (Table 1 and Figure 5). Very high NTG values suggest extensive sand development, which can often be weakly consolidated and prone to sand production under stress (Phillips, 2007). Porosity (Φ) values in ANY field range between 0.25 and 0.29, indicating moderate to high void spaces in the reservoir rock. High porosity often weakens the rock matrix, increasing the risk of grain detachment during hydrocarbon production (Baker *et al.*, 2015) (Table 1). The Water Saturation (Sw) ranges from 0.10 to 0.40 (Table 1). The elevated SW weakens the reservoir rock by increasing pore pressure and reducing effective stress, making these reservoirs more vulnerable to sand production (Saboorian-Jooybari *et al.*, 2023). Permeability values range from 0.80 D to 1.10 D. High permeability correlates with efficient fluid flow but may also indicate loose grain packing, further increasing susceptibility to sand detachment (Baker *et al.*, 2015).

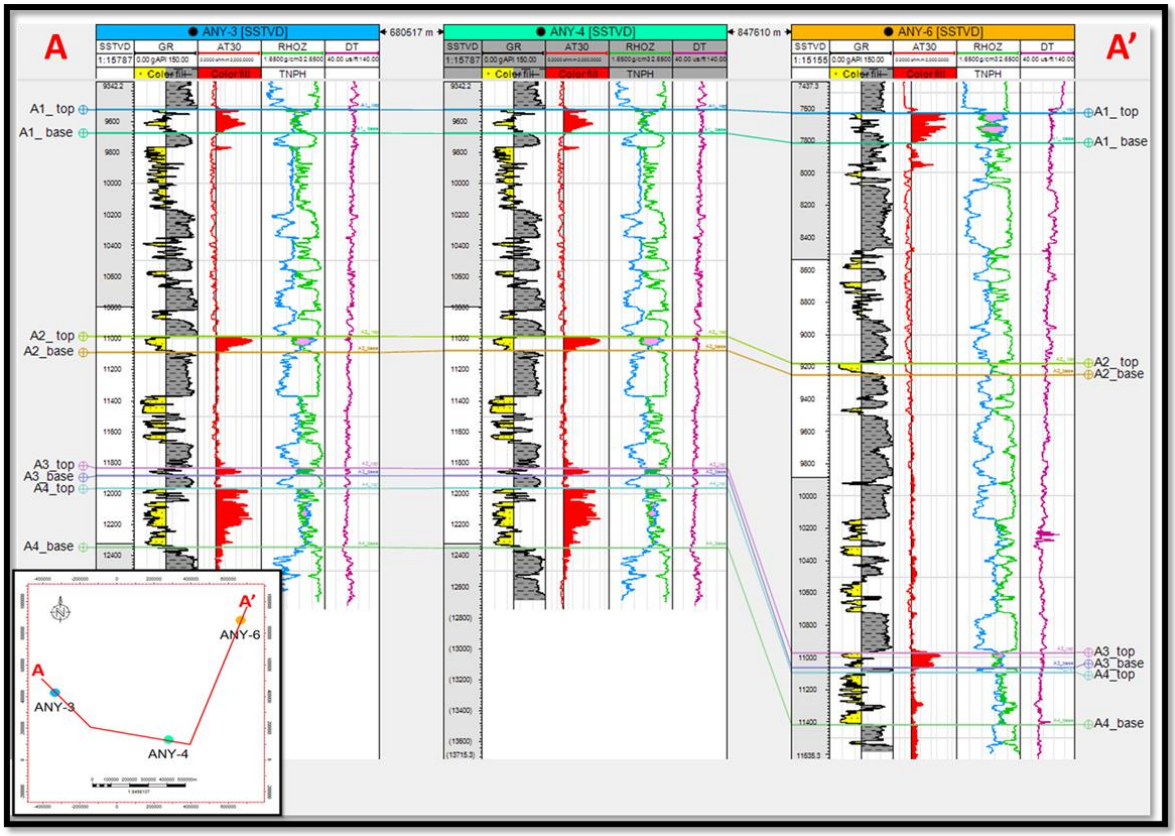

Figure 4: Well correlation panel showing delineated reservoirs.

From the petrophysical results shown in Table 1 and Figure 5, A1 RES shows no potential for sand production. The porosity (ϕ) value of 0.27 is below the required threshold of >0.30, and the permeability of >0.90 D does not meet the minimum required value of >2.0 D. Similarly, the water saturation (Sw) and NTG are significantly lower, at 0.10 and 0.38, respectively (Saboorian-Jooybari *et. al.*, 2023). These suboptimal values indicate that A1 RES does not meet the conditions necessary for sand production.

In A2 RES, the porosity (ϕ) is 0.29, falling just below the threshold, while the permeability is 1.10 D, which is also insufficient. The water saturation of 0.38 and NTG of 0.70 further confirm that this well does not exhibit favorable conditions for sand production. Similarly, A3 RES has a porosity (ϕ) of 0.28, and the permeability is 0.85 D, both of which are below elevated levels of sanding. The water saturation (Sw) of 0.14 and NTG of 0.47 are also far from the required thresholds. Consequently, Well A3 does not demonstrate any potential for sand production. A4 RES exhibits a similar trend of unfavorable conditions. The porosity (ϕ) is 0.25, and the permeability is 0.80 D, both of which are below the required thresholds. Additionally, the water saturation of 0.40 and NTG of 0.66 fall short of the necessary cutoffs. Thus, Well A4 also does not meet the criteria for sand production

Table 1: Computed petrophysical results for ANY field

WELL	NTG *(frac.)*	Phi *(frac.)*	Sw *(frac.)*	Perm *(D)*
A1	0.38	0.27	0.10	0.90
A2	0.70	0.29	0.38	1.10
A3	0.47	0.28	0.14	0.85
A4	0.66	0.25	0.40	0.80

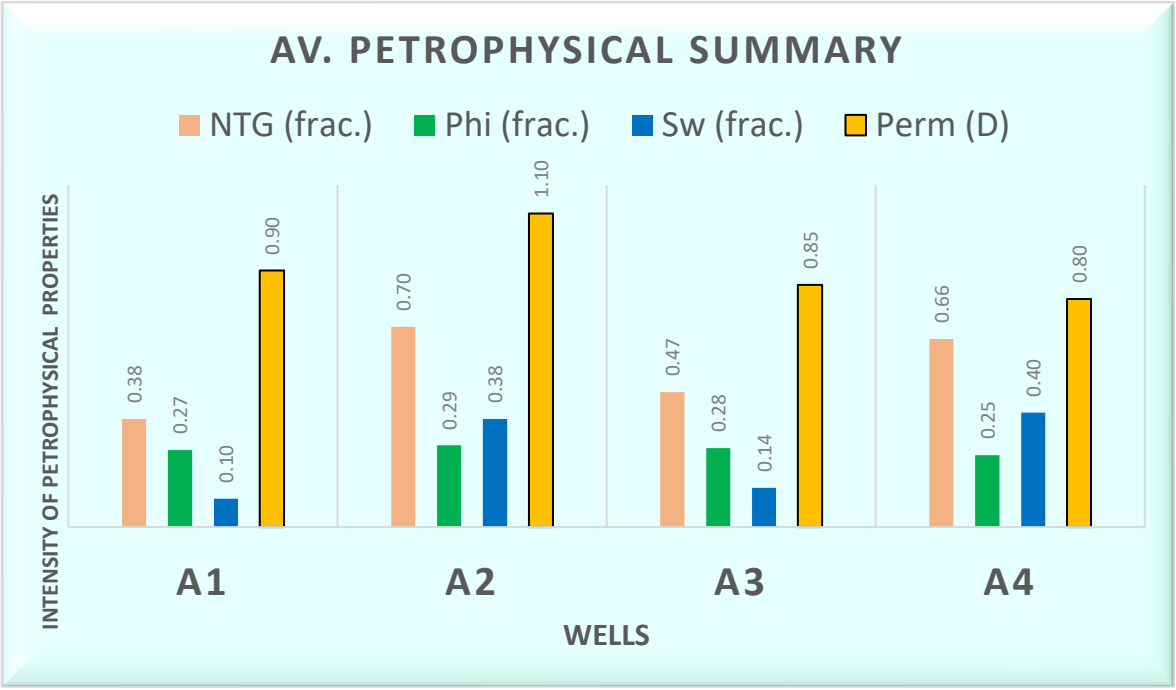

Figure 5: Comparative plot of petrophysical properties across ANY field.

4.4 Seismic Analysis

4.4.1 Synthetic Seismogram

The synthetic seismogram (Figure 6) ensures a fundamental link between well data and seismic data, and it is the main tool that allows geological picks from the well to be associated with seismic. This was done using the check shot data, and Figure 6 shows good ties between events on the well, the field seismic, and the synthetic seismic.

4.4.2 Fault Interpretation

The structural framework was done by picking assigned faults on inline sections of the seismic volume. These faults are represented on the seismic sections as discontinuous reflection along a preferred orientation of reflectors or as distortion of amplitude around the fault zones. A total of thirty-five faults were identified on the inline (Figure 7), some extending through the extent of the field known as major regional growth faults and a few antithetic faults

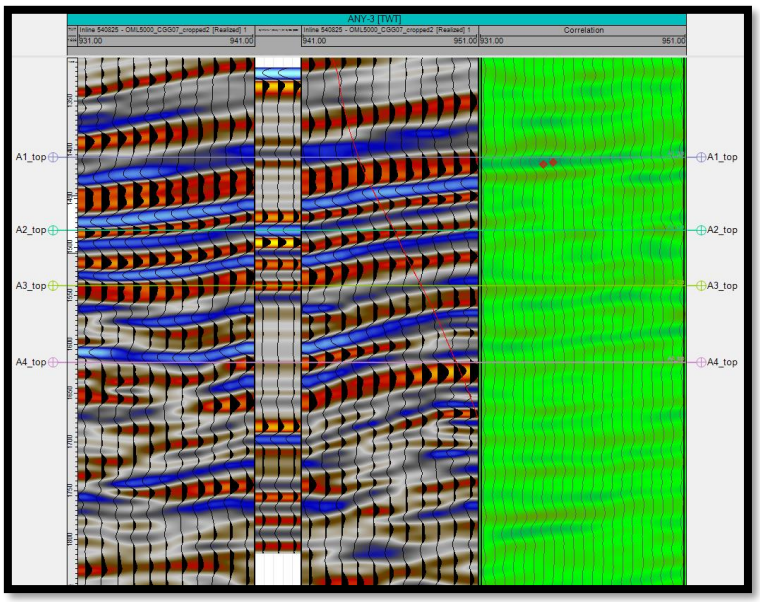

Figure 6: Synthetic Seismogram generated for ANY field

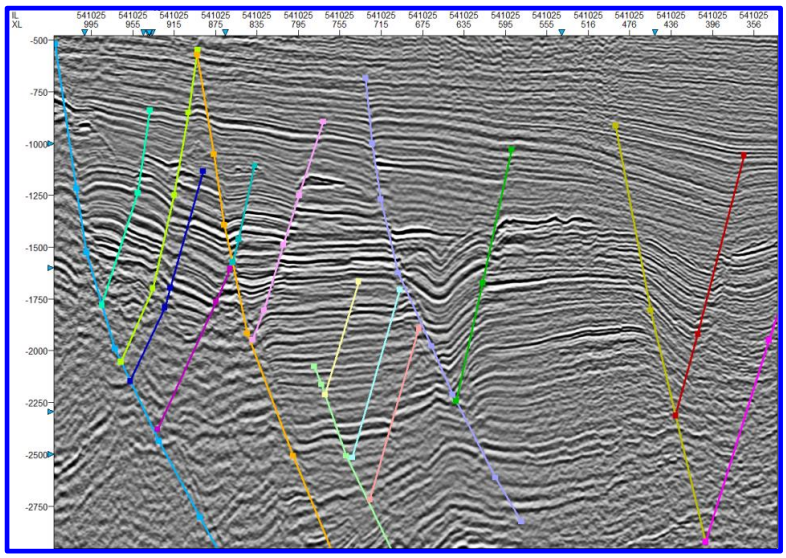

Figure 7: Interpreted faults displayed on Seismic inline 506850

4.4.3 Horizon Interpretation

In order to understand the subsurface geology and structural trend for possible hydrocarbon accumulation, seismic and well data were tied. Based on the seismic-to-well ties, four major horizons identified on the well logs were picked and interpreted across the seismic survey. The four hydrocarbon-bearing sand units (A1, A2, A3, and A4) within the Agbada Formation, which are the interval of interest, were mapped every 5 milliseconds within the seismic section (Figure 8).

4.4.4 Time Surface

Time contour maps showing the most accurate representative geology of the A1-A4 reservoir are presented in Figure 9. The maps show the major faults that formed the closure that contributes to the accumulation of hydrocarbon in the field.

4.4.5 Depth Surface

The resultant depth residual values generated using the 2nd order polynomial velocity model (Figure 10) were used for converting reservoirs from time to depth because they have the least residuals. The depth-converted reservoir surface is presented in Figure 11 for the second-order polynomial velocity function. The depth structure maps reveal that the reservoirs are anticlinal and fault supported.

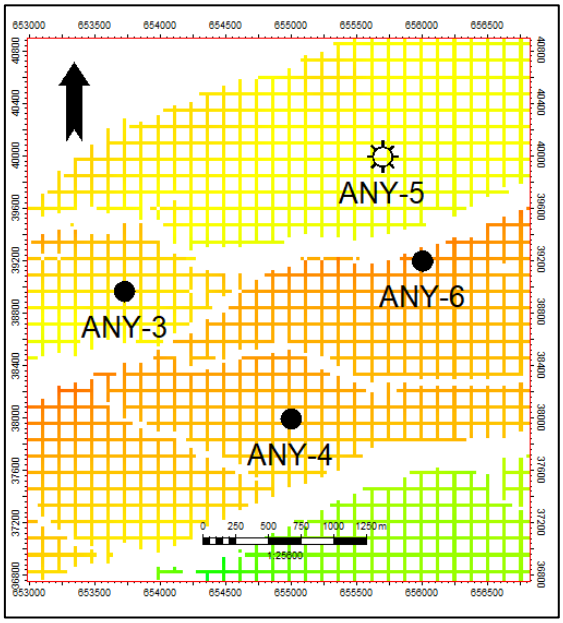

Figure 8: Mapped Seeded horizon (5x5)

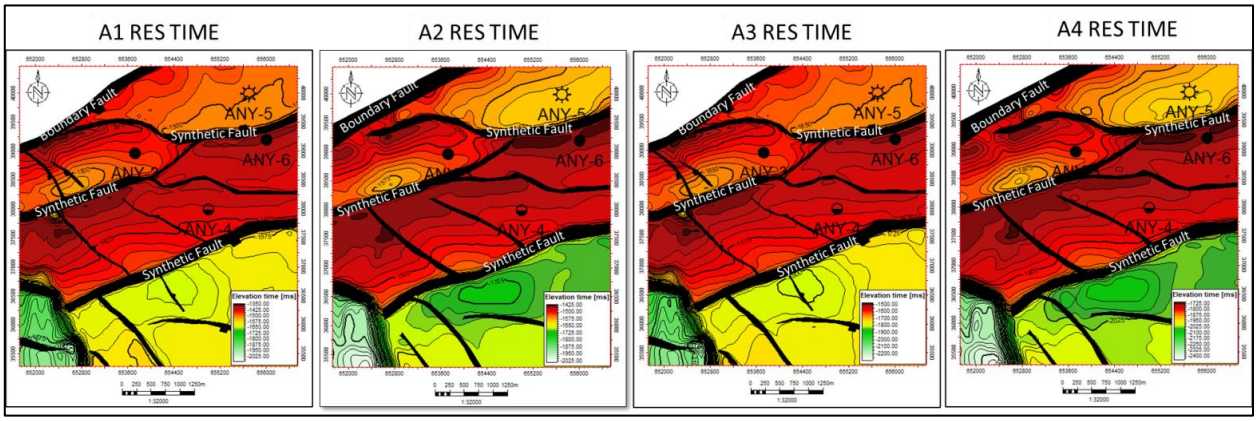

Figure 9: Time Maps for A1-A4 reservoir showing the fault structures of the field

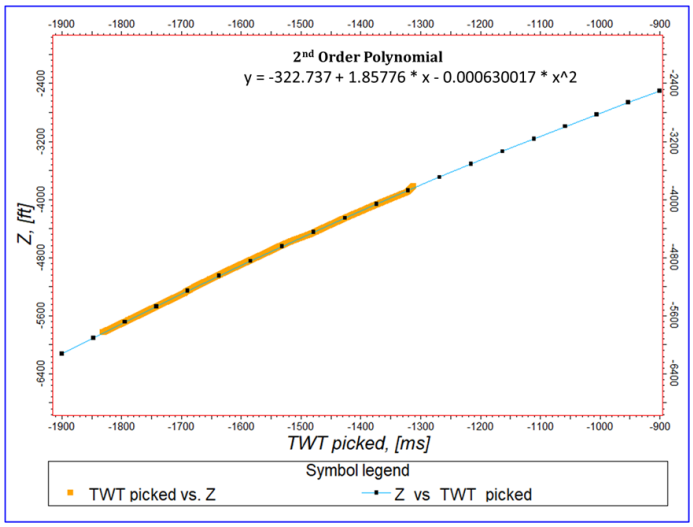

Figure 10: Velocity model showing the time to depth relationship

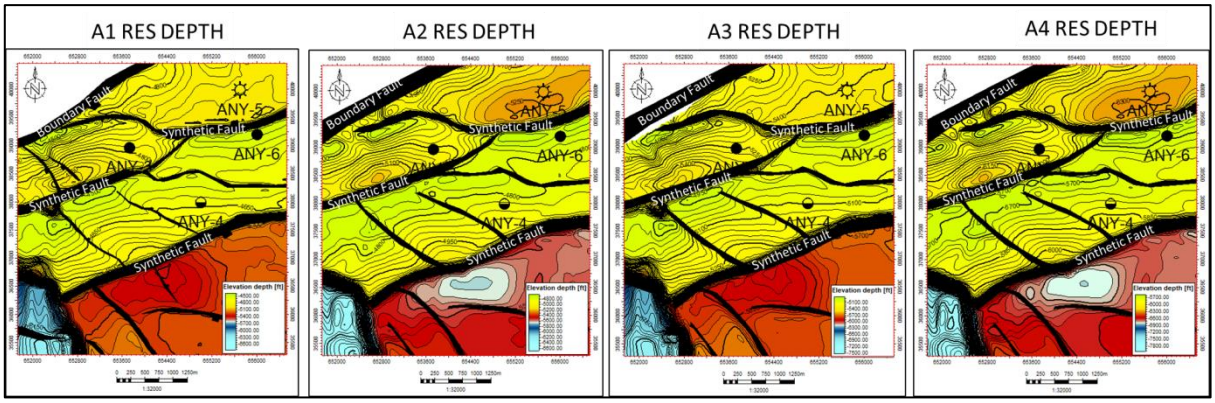

Figure 11: Depth Maps for A1-A4 reservoirs showing the fault structures of the field

The structural framework showing different oriented growth faults is presented in Figure 9 (Time Map) and Figure 11 (Depth Maps). The faults were observed to be elongate, generally trending northwest to southeast. The field is divided into three fault blocks by three major synthetic faults trending in a north-west–south-east direction (Figure 11). The sub-faults are antithetic trends in the northeast-southwest direction and provide secondary traps for the reservoirs (Figure 4.11). The faults observed were predominantly listric normal growth faults, with a sub-parallel relationship (**Figure** 11). The wells drilled in the field targeted the horstal

structure (Figure 11). The field illustrates an extensional collapse of the passive continental margins. Roll-over anticlines were formed as a product of the deformation of deposited sediments at the downthrown block of major faults. The reservoirs in the seismic survey were observed to be rollover anticline structures, bounded by the closure of the boundary synthetic faults, which provided the structural dip closure (trap) responsible for hydrocarbon accumulation in the field (Figure 11). The numerous fault blocks formed due to extensive faulting. has compartmentalize the reservoirs, leading to variations in pressure, fluid properties, and stress regimes across different blocks. Such disparities can affect rock stability and, consequently, the propensity for sand production (Opara & Onuoha, 2009). Furthermore, the juxtaposition of rock layers with differing properties due to fault movements can result in zones of weakly consolidated sands adjacent to more competent rocks, increasing the likelihood of sand production in the weaker zones (Weber & Daukoru, 1975). The resultant depth residual values generated using the 2nd order polynomial velocity model (Figure 10) were used for converting reservoirs from time to depth because they have the least residuals. The depth-converted reservoir surface is presented in Figure 11 for the second-order polynomial velocity function. The depth structure maps reveal that the reservoirs are anticlinal and fault supported.

4.5 Geomechanical Analysis

With a mean value of Poisson ratio, bulk modulus, shear modulus, Young's modulus, and unconfined compression strength for the ANY reservoirs as shown in Tables 2-5, the formation can withstand a force of compression without shattering or failing entirely. It indicates that reservoirs will require a greater vertical stress or pressure to undergo deformation. In a hydraulic fracture process, the shale forms seal rocks to the fault zone because these qualities also make the shale fracture stimulation barriers. When a series of sandstones with high porosity is divided by impermeable shales, this is one of the main reasons for hydrocarbon reservoir compartmentalization (Ortoleva, 1994). Additionally, the results indicate that reservoirs with moderate porosity can make it stiffer and denser. Since pores are among the weakest and the most brittle features of rocks, an increase in porosity results in a failure in the elastic moduli and rock strength of reservoir units. Figures 13-16 show the comparative plots of geomechanical parameters across the four reservoirs, respectively. With a mean value of Poisson ratio, bulk modulus, shear modulus, Young's modulus, and unconfined compression strength for the ANY reservoirs as shown in Tables 2-5, the formation can withstand a force of compression without shattering or failing entirely. It indicates that reservoirs require a greater vertical stress or pressure to undergo deformation. In a hydraulic fracture process, the shale forms seal rocks to the fault zone because these qualities also make the shale fracture stimulation barriers. When a series of sandstones with high porosity is divided by impermeable shales, this is one of the main reasons for hydrocarbon reservoir compartmentalization (Ortoleva, 1994). Additionally, the results indicate that reservoirs with moderate porosity can make it stiffer and denser. Since pores are among the weakest and the most brittle features of rocks, an increase in porosity results result in a failure in the elastic moduli and rock strength of reservoir units. Figures 13-16 show the comparative plots of geomechanical parameters across the four reservoirs, respectively.

4.6 Sand Prediction

Predicting whether a well will produce fluids without producing sand has been the goal of many well completion engineers and research projects. There are a number of analytical techniques and guidelines to assist in determining if sand control is necessary.

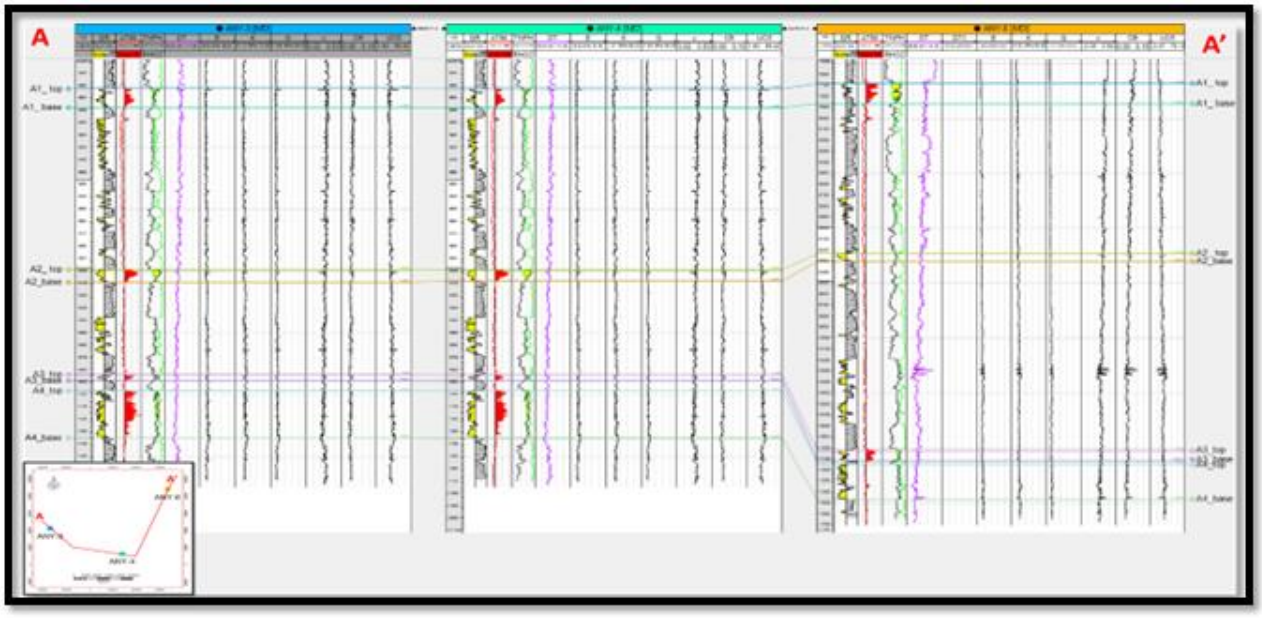

Figure 12: Geomechanical Property Logs Showing Lithology, Poisson Ratio (V), Bulk Modulus (Kb), Shear Modulus (G), Young Modulus (E), Bulk Compressibility (Cb) Unconfined Compression Strength (UCS) of the ANY field.

Table 2: Computed Geomechanical properties for A1 reservoir interval

A1 RES										
WELL	DT	BULK_M	POIS	SH_MOD	Y_MOD	UCS	CB	G/Cb	B	SI
	us/ft	*MPA*		*MPa*	*MPa*	*MPa*	*Mpa-1*	*$10^{12}psi^2$*	*10^6 psi²*	*10^{12} psi²*
ANY-3	92.903	15.857	0.33	6.272	16.581	22.927	0.64	9.8	16.581	99.4551
ANY-4	92.899	15.843	0.328	6.253	16.536	22.928	0.64	9.7703	16.536	99.06628
ANY-6	96.864	14.181	0.342	5.016	13.455	21.501	0.71	7.0648	13.455	71.1319
AVERAGE	94.222	15.294	0.333	5.847	15.524	22.452	0.663	8.878	15.524	89.884
STAND_DEV	2.288	0.964	0.008	0.720	1.792	0.824	0.040	1.571	1.792	16.241
CV(%)	2.428	6.301	2.272	12.309	11.543	3.668	6.093	17.691	11.543	18.069

In the present study, the two most sophisticated approaches to predicting sand production are estimating petrophysical properties from well logs and the use of geomechanical numerical models developed to analyze sand prediction/fluid flow through the reservoir in relation to the formation strength. These approaches are considered a valid solution that can provide results with a reasonable level of accuracy in predicting sanding in a reservoir (Ehsan & Ebrahim, 2015). The prediction required is on a reservoir-by-reservoir basis.

Five methods were used in predicting sand production. These methods are as follows:

1. Porosity method
2. Acoustic wave travel time
3. Sand production index (B)
4. Schlumberger sand production index (SI)
5. Shear modulus to bulk compressibility ratio

4.6.1 Prediction of Sanding using the Porosity Method

The porosity values of ANY field in reservoirs A1, A2, A3, and A4 are 0.27%, 0.29%, 0.28%, and 0.25%, respectively, as shown in Table 1.

The porosity of a formation is s sued as a guideline as to whether sand control is needed. If the formation porosity is greater than 30%, the probability of the need for sand control is high because of inadequate cementation. A formation porosity of less than 20% indicates that the formation is consolidated and there may be no sand production in the formation/reservoir (Ehsan & Ebrahim, 2015). The porosity values in the field are below the threshold value of

>30% for sand production from a reservoir (Ehsan & Ebrahim & Ebrahim, 2015). Based on the calculated porosity values from the four reservoirs, sanding is not likely to occur in the field.

4.6.2 Prediction of Sanding using Acoustic Wave Travel Time Method ΔTc

The average acoustic wave travel time values for the four reservoirs in ANY field range from 77.82 to 94.22 $\mu s/ft$, as shown in Table 2 to 5. Based on the Δ**TC** method **C** method if sonic compressive time is greater than 104 $\mu s/ft$, the formation will produce sand. The result obtained from this study is below the value of 104 $\mu s/ft$ for sand production to occur, and so the reservoir is not likely to produce sand (Ehsan *et al.*, 2015).

4.6.3 Prediction of Sanding using Sand Production Index (B)

In this research, predicting sanding using the B shows that the average values the sand production index obtained in the reservoirs fall between $15.52 \times 10^6 - 29.26 \times 10^6 psi$ as shown in Tables 2 to 5. A sand control technique is required in a reservoir when B in the reservoir is less than $2.9 \times 10^6 psi$ (Ehsan et al., 2015). Research carried out in Egyptian wells by Bianlong *et al.* (2013) obtained a B of $0.73 \times 10^6 psi$ in their reservoir of study. They concluded that sanding was likely to occur. Comparatively, the study shows that sanding is not likely to occur in the study area.

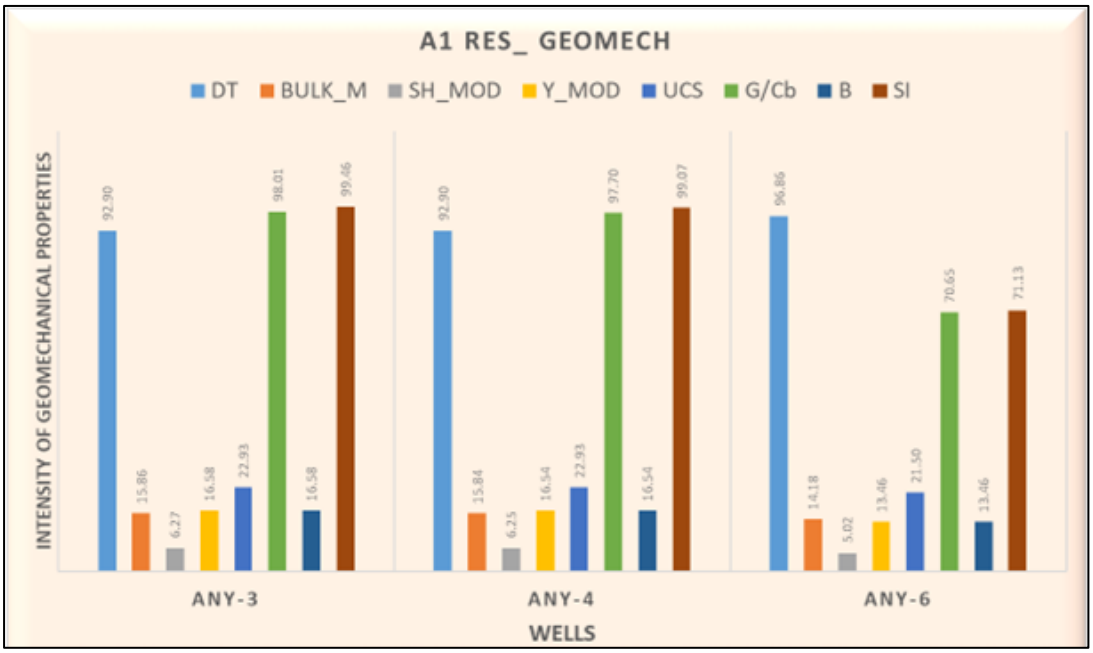

Figure 13: Comparative plot of Geomechanical properties across A1 Res interval.

Table 3: Computed Geomechanical properties for A2 reservoir interval

A2 RES										
WELL	DT	BULK_M	POIS	SH_MOD	Y_MOD	UCS	CB	G/Cb	B	SI
	us/ft	*MPA*		*MPa*	*MPa*	*MPa*	*Mpa-1*	10^{12} *psi*^{2}	10^6 *psi*^{2}	10^{12} *psi*^{2}
ANY-3	85.529	17.702	0.301	8.176	21.231	25.702	0.57	14.344	21.231	144.7316
ANY-4	84.865	18.423	0.298	8.644	22.403	25.979	0.55	15.716	22.403	159.2484
ANY-6	86.942	17.406	0.306	7.806	20.346	25.141	0.7	11.151	20.346	135.8712
AVERAGE	**85.779**	**17.844**	**0.302**	**8.209**	**21.327**	**25.607**	**0.607**	**13.737**	**21.327**	**146.617**
STAND_DEV	**1.061**	**0.523**	**0.004**	**0.420**	**1.032**	**0.427**	**0.081**	**2.342**	**1.032**	**11.802**
CV(%)	**1.237**	**2.932**	**1.340**	**5.116**	**4.838**	**1.667**	**13.425**	**17.050**	**4.838**	**8.050**

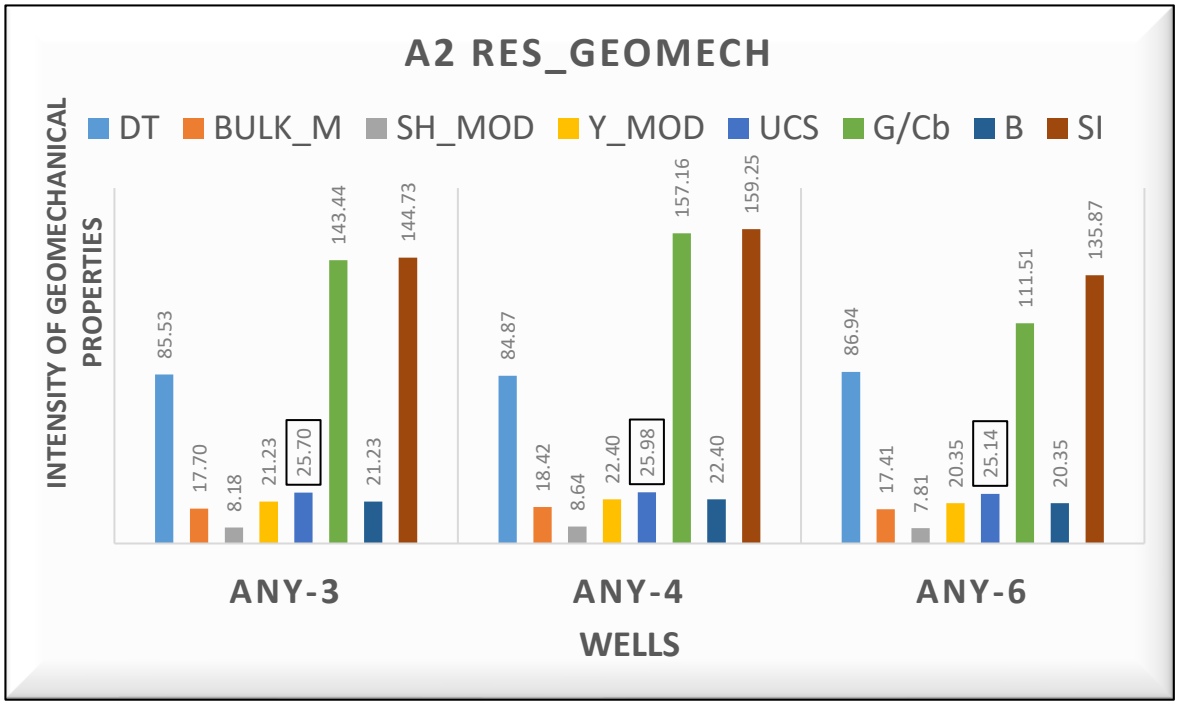

Figure 14: Comparative plot of Geomechanical properties across A2 Res interval

Table 4: Computed Geomechanical properties for A3 reservoir interval

A3 RES										
WELL	DT	BULK_M	POIS	SH_MOD	Y_MOD	UCS	CB	G/Cb	B	SI
	us/ft	MPA		MPa	MPa	MPa	Mpa-1	10^{12} psi^2	10^{6} psi^2	10^{12} psi^2
ANY-3	81.331	19.801	0.283	13.76	34.49	30.832	0.51	26.9804	34.49	272.462
ANY-4	80.491	20.403	0.28	10.644	27.176	27.956	0.5	21.288	27.176	217.17
ANY-6	80.849	19.275	0.282	9.908	25.359	27.752	0.52	19.0538	25.359	190.977
AVERAGE	80.89	19.826	0.282	11.437	29.01	28.85	0.51	22.44	29.01	226.9
STAND_DEV	0.422	0.5644	0.002	2.0449	4.833	1.722	0.01	4.087	4.833	41.6
CV(%)	0.521	2.8469	0.542	17.879	16.66	5.971	1.961	18.21	16.66	18.34

4.6.4 Prediction of Sanding using Schlumberger Sand Production Index (SPI)

From this research, predicting sanding using the Schlumberger sand production index (S/I) shows that the average values of the Schlumberger sand production index obtained in the reservoirs fall between 89.8 × 10^{12} and 242.0 × 10^{12} psi², as shown in Tables 2 to 5. A sand control technique is required in a reservoir when the Schlumberger sand production index in the reservoir is less than 1.24 × $10^{12} psi^2$ (Ehsan & Ebrahim, 2015). Based on the results obtained in this research using the Schlumberger production index (S/I), it is observed that sanding is not likely to occur in the reservoirs. In their research, Bianlong *et al.* (2013) used the Schlumberger sand production index to predict if their reservoir is likely to produce sand. The values they obtained were less than 1.24 × $10^{12} psi^2$, which indicated that the reservoir was likely to produce sand.

4.6.5 Prediction of Sanding using Shear Modulus to Bulk Compressibility Ratio (G/C_b)

Results of G/$C_b$as shown in Tables 2 to 5 reveal that the analytical average values of G/$C_b$obtained range from 8.877 × 10^{12} to 23.95 × $10^{12} psi^2$.

According to Tixier *et al.* (1975), the threshold values for sanding using G/C_b are <0.8 × $10^{12} psi2$. The values obtained from the study

are far above the threshold value. Thus, indicating that the reservoirs are not likely to produce sands during production. Researchers such as Ehsan and Ebrahim (2015) used G/C_b to estimate sanding in their studies; the values they calculated were higher than the threshold values for sanding, indicating that their reservoirs did not produce sand.

4.7 Analysis of the Populated Sand Production Parameters on the Reservoir Surfaces

Figures 17 to 20 show the distribution of B, SPI, and shear modulus to bulk compressibility ratio (G/Cb), respectively, across the reservoir surface. Analysis of these maps shows that a greater percentage of the reservoir interval across the field is not prone to sanding during wellbore and production.

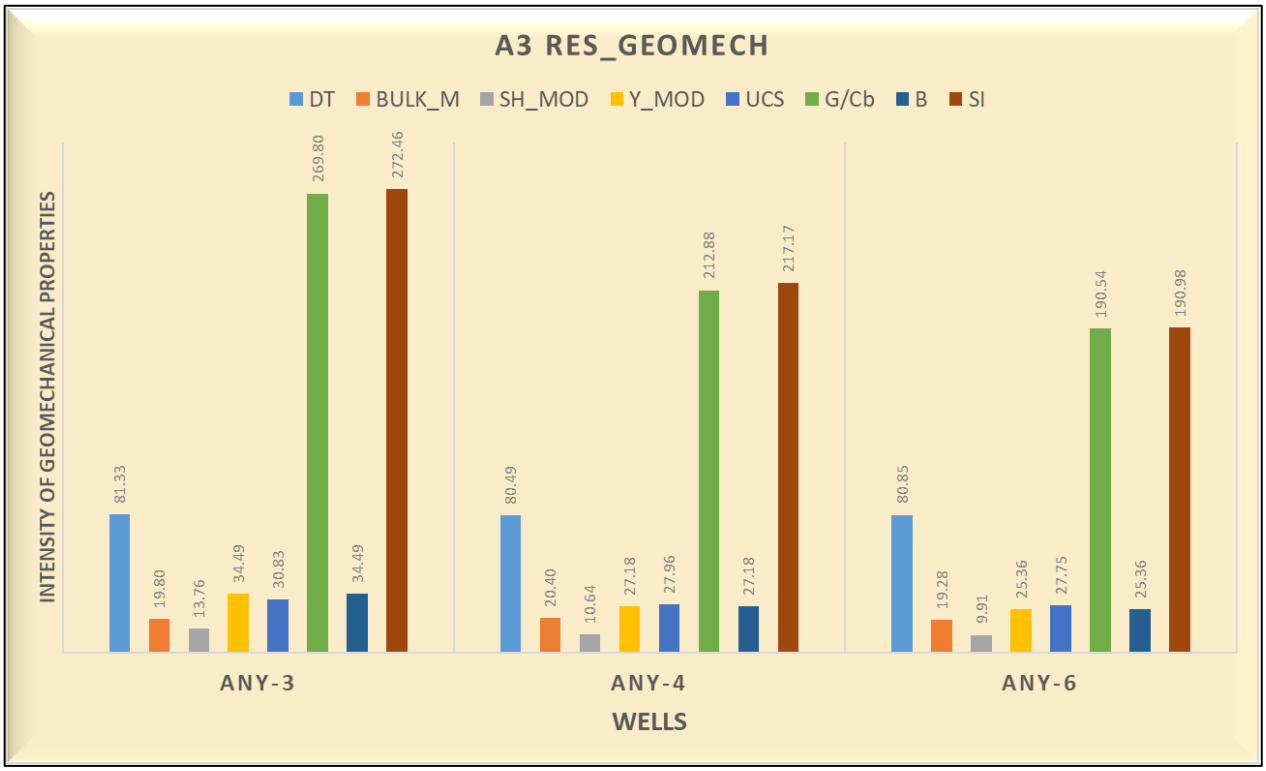

Figure 15: Comparative plot of Geomechanical properties across A4 Res interval.

Table 5: Computed Geomechanical properties for A4 reservoir interval.

A4 RES										
WELL	DT	BULK_M	POIS	SH_MOD	Y_MOD	UCS	CB	G/Cb	B	SI
	us/ft	*MPA*		*MPa*	*MPa*	*MPa*	*Mpa-1*	*10^{12} psi^2*	*10^{6} psi^2*	*10^{12} psi^2*
ANY-3	78.67	20.594	0.272	11.165	28.347	28.808	0.49	22.7857	28.347	229.932
ANY-4	78.695	20.562	0.272	11.132	28.27	28.793	0.49	22.7184	28.27	228.896
ANY-6	76.109	21.56	0.26	12.386	31.167	30.103	0.47	26.3532	31.167	267.042
AVERAGE	**77.82**	**20.905**	**0.268**	**11.561**	**29.26**	**29.23**	**0.483**	**23.95**	**29.26**	**242**
STAND_DEV	**1.486**	**0.5672**	**0.007**	**0.7147**	**1.651**	**0.752**	**0.012**	**2.079**	**1.651**	**21.73**
CV(%)	**1.909**	**2.7131**	**2.585**	**6.1817**	**5.642**	**2.572**	**2.389**	**8.681**	**5.642**	**8.981**

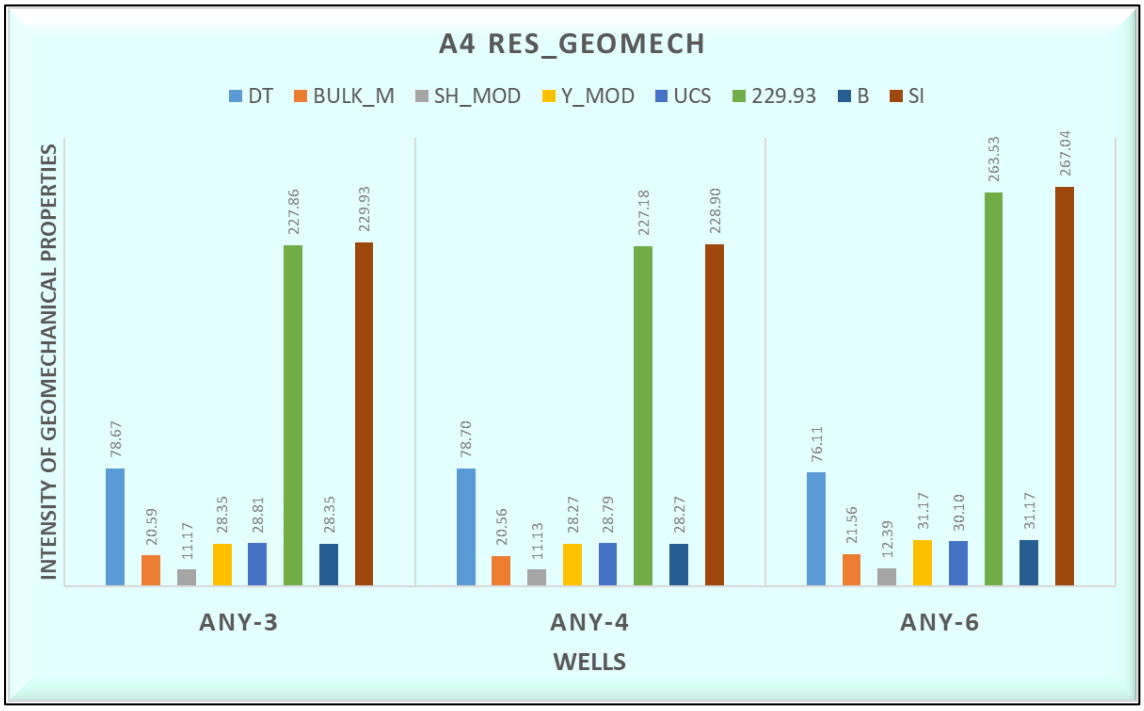

Figure 16: Comparative plot of Geomechanical properties across A4 Res interval.

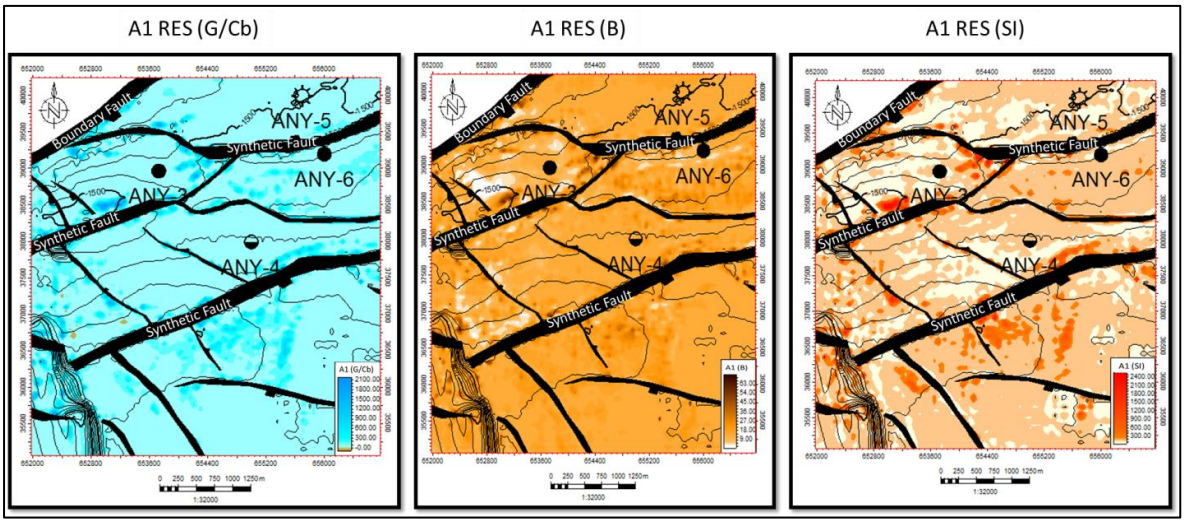

Figure 17: Populated sand production parameters across the A1 RES interval.

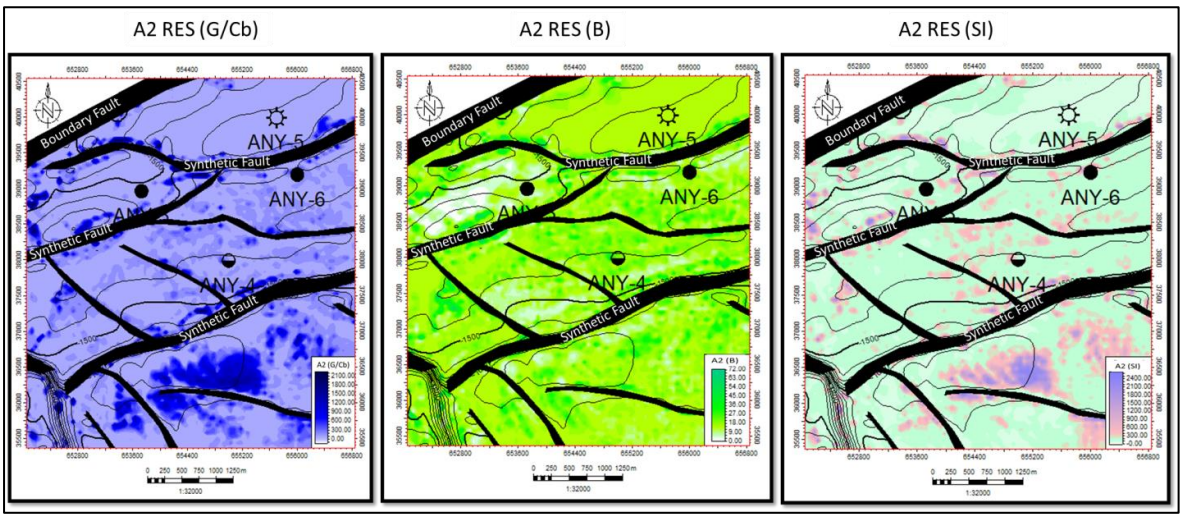

Figure 18: Populated sand production parameters across the A2 RES interval.

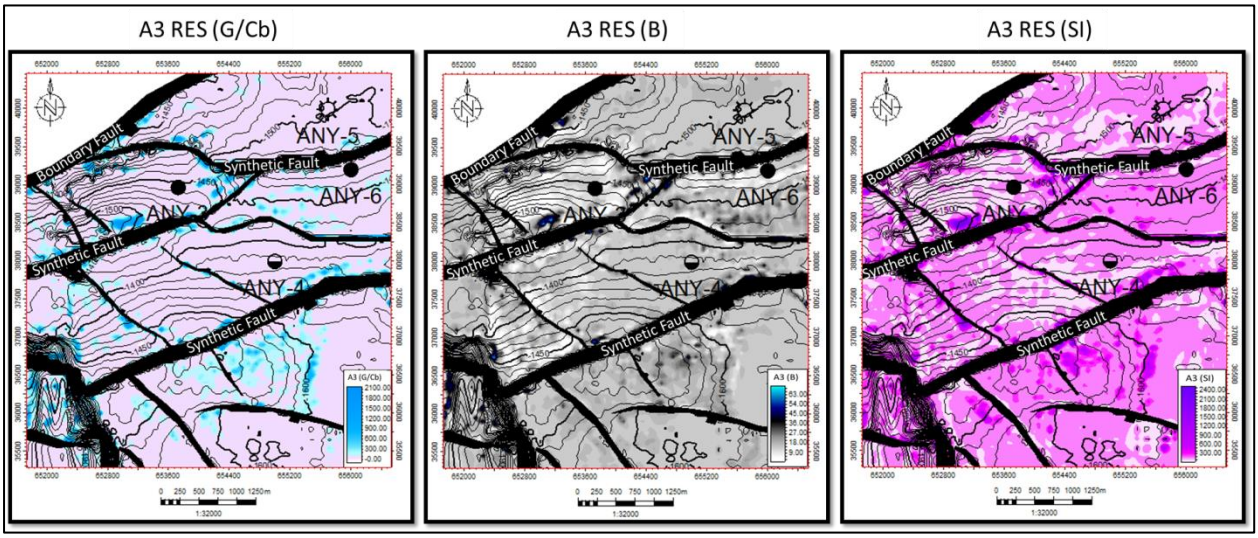

Figure 19: Populated sand production parameters across the A3 RES interval.

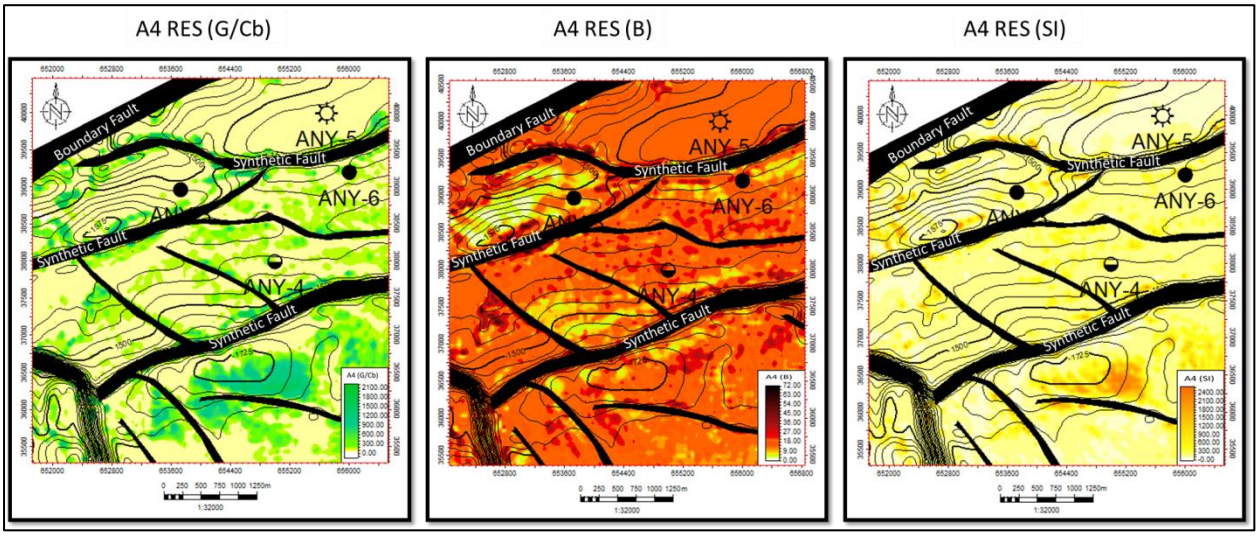

Figure 20: Populated sand production parameters across the A4 RES interval

5. Conclusion

Datasets from ANY field were analyzed for petrophysical and geomechanical properties of the study area. These properties were used to derive various parameters that were used to predict the likelihood of the occurrence of sand in a reservoir. Five sand production methods (porosity, acoustic wave travel time, sand production index (B), Schlumberger sand production index (SPI), shear modulus to bulk compressibility ratio (G/Cb)) were used in predicting sanding in the reservoirs of interest. From the results of this research, the following conclusions are reached:

- It is observed that none of the reservoirs is likely to produce sand during drilling based on the petrophysical parameters.
- The reservoirs were consolidated for sanding to occur, as shown from the porosity/ permeability values of the reservoirs.
- Different methods (porosity, acoustic wave travel time, sand production index (B), Schlumberger sand production index (SPI), shear modulus to bulk compressibility ratio) of sand production prediction were used in this research work to obtain accurate results, and the results show that the reservoirs were highly compacted and consolidated and would not produce sanding during production; therefore, the field will not

encounter flow problems during production petrophysically.

This study evaluates the geomechanical and petrophysical parameters of the field as a basis for sand production. It is important to note that several factors can contribute to sand production and flow problems in a reservoir. High flow rates and pressure drawdown, for instance, can destabilize the formation due to excessive production rates or sudden changes in reservoir pressure, leading to sand failure. Water breakthrough and water cutting also play a significant role, as water influx into the reservoir reduces capillary forces holding sand grains together, thereby increasing sand production. Additionally, gas expansion and depletion effects, where rapid gas expansion due to pressure depletion weakens the rock structure, can further promote sand failure. Poor wellbore design and casing integrity issues, such as inadequate gravel packs, screens, or perforation strategies, contribute to sand failure, while high production-induced stresses accelerate rock failure by increasing stress concentration around the wellbore.

To mitigate sanding throughout the lifespan of a well during production, it is recommended that well logs be utilized to predict the likelihood of sanding during well development, allowing for the formulation and application of appropriate control or management strategies in well design. Furthermore, future research should focus on integrating additional data types, such as core and production data, to refine predictive models. The application of advanced machine learning techniques, including deep learning, may enhance model accuracy. Additionally, collaboration between industry and academia is crucial for validating and implementing these predictive models in field operations.

References

Adeoye, T. O., Olatunji, B., & Olawale, D. (2020). Challenges and management of sand production in the Niger Delta reservoirs. Journal of Petroleum Exploration and Production Technology.

Akpan, A.S., Obiora, D.N., Okeke, F.N., Ibuot, J.C., and George, N.J., 2020a. Influence of wavelet phase rotation on post stack model based seismic inversion: A case study of X-field Niger Delta, Nigeria. Journal of Petroleum and Gas Engineering, UK, 11 (1), Pp. 57– 67. https:// doi.org/ 10.5897/ JPGE219.0320.

Akpan, A.S., Okeke, F.N., Obiora, D.N., and George, N.J., 2020b. Modelling and mapping hydrocarbon saturated sand reservoir using Poisson's impedance (PI) inversion: A case study of Bonna field Niger Delta Swamp Depobelt, Nigeria. Journal of Petroleum Exploration and Production Technology

Akpan, M.J., George, N.J., Ekanem, A.M., and Nathaniel, E.U., 2022. Utilizing Probabilistic Neural Network for Reservoir Assessment: A Case Study from an Onshore Niger Delta Field. Researchers Journal of Science and Technology, 2 (3), Pp. 55–67.

Akpan, M.J., George, N.J., Ekanem, A.M., Ekong, U.N., 2022. Ekong Petrophysical appraisal and 3D structural interpretation of reservoirs in an Onshore Niger Delta Field, Southeastern Nigeria. International Journal of Energy and Water Resources, https://doi.org/10.-1007/s42108-022-00218-9.

Barefield, E., & Shakoor, A. (2006). *The effect of degree of saturation on the unconfined compressive strength of selected sandstones.* In *Proceedings of the International Association for Engineering Geology and the*

Environment (IAEG) 2006 Conference (Paper No. 606). The Geological Society of London.

Bianlong, Z., Ma, D., Li, L., Juncheng, H. (2013). Application of Logging Data in Predicting Sand Production in Oilfield. *Egyptian Journal of Petroleum, 18,* 6173-6180.

Ebong, S.T., Aniekan, M., Ekanem, A.M., George, N.J., (2023). Reservoir Characterisation Using Seismic Inversion Techniques for Mapping of Prospects. Researchers Journal of Science and Technology, 3 (1), Pp. 1 – 13.

Ehsan K. & Ebrahim R. (2015). Sand production prediction using ratio of shear modulus to bulk compressibility (case study). *Egyptian Journal of Petroleum Volume 24, Issue 2, June 2015, Pages 113-118.*

George, N.J., Umoh, J.A., Ekanem, A.M., Agbasi O.E. Asfahani, J. Thomas J.E. (2022). Geophysical-laboratory data integration for estimation of groundwater volumetric reserve of a coastal hinterland through optimized interpolation of interconnected geo-pore architecture. *J Coast Conserv* 26, 56. https://doi.org/10.1007/s11852-022-00902-2

Horsfall, O.I., Akpan M.J. & George, N.J. (2024) Reservoir characterization of GABO field in the Niger Delta Basin using facies and petrophysical analyses, Results in Earth Sciences, Vol. 2,100038, https://doi.org/10.1016/j.r-ines.2024.100038

Ibrahim, S., Ehirim, C. N., & Etim, A. A. (2021). Geomechanical assessment of sand production in the Niger Delta. *Journal of Petroleum Exploration and Production Technology.*

Ogagarue, D.O. (2008). Localized VP − VS Relationships from the Niger Delta Sediments. *The Pacific Journal of Science and Technology. 9 (2). 558 - 561.*

Ortoleva, P., Ed. (1994). Basin Compartments and Seal rocks. *Tulsa. American Association of Petroleum Geologists.*

Osia, S. I., Ajibola, A. & Enemuoh, E. E. (2020). Predictive modeling of sand production in Niger Delta fields. *SPE Nigeria Annual International Conference and Exhibition.*

Santarelli, F. J., & Carminati, S. (1995). Predicting sand production in poorly consolidated reservoirs. *Journal of Petroleum Science and Engineering.*

Short, K. C., & Stauble, A. J. (1967). Outline of Geology of Niger Delta. *AAPG Bulletin*, 51(5), 761–779.

Tixier, M.P. Loveless, G.W. & Anderson, R.X. (1975) Estimation of the formation strength from the mechanical properties log. *Journal of Petroleum Technology, 27, 283-293.*

Tuttle, M. L. W., Charpentier, R. R., & Brownfield, M. E. (1999). The Niger Delta Petroleum System*: Niger Delta Province, Nigeria, Cameroon, and Equatorial Guinea, Africa (Open-File Report 99-50-H). U.S. Geological Survey*

Weber, K. J., &Daukoru, E. M. (1975). Petroleum Geology of the Niger Delta. *Proceedings of the Ninth World*

Petroleum Congress, Volume 2, Geology, 209-221.

Vail, P. R. (1987). Seismic stratigraphy interpretation procedure. *AAPG Studies in Geology*, 27, 1–10.

Baker, R., Corbett, P., & Jiang, Z. (2015). Some rules of thumb for porosity cut-offs. *ResearchGate*. Retrieved from https://www.researchgate.net/figure/Some-rules-of-thumb-for-porosity-cut-offs-Baker-et-al-2015_tbl1_370141923

Phillips, S. (2007). Improving net–to-gross reservoir estimation with small scale heterogeneity analysis. *Search and Discovery Article #40352*. Retrieved from https://www.search and discovery-.com/documents/2007/07079phillips/images/phillips.pdf

Saboorian-Jooybari, H., & Kazemi, H. (2023). A comprehensive methodology for reservoir cut-off determination. *Journal of Petroleum Exploration and Production Technology*, 13, 123–145. https://doi.org/10.1007/s13202-023-01636-z

Opara, A. I., & Onuoha, K. M. (2009). Evaluation of formation susceptibility and sand production potential in Niger Delta oil reservoirs. *Journal of Petroleum Science and Engineering, 70*(3–4), 179–185.